Non-linear regularized decomposition of spectral x-ray projection images

Nicolas Ducros, Simon Rit, Bruno Sixou, Françoise Peyrin

Non-linear regularized decomposition of spectral x-ray projection images

Nicolas Ducros*, Simon Rit, Bruno Sixou and Françoise Peyrin

***Abstract*—Spectral computed tomography (CT) exploits measurements from x-rays with different energies to obtain the 3D description of the patient in a material basis. It requires to solve two subproblems, namely the material decomposition and the tomographic reconstruction problems, either sequentially or jointly. In this work, we address the material decomposition problem, which an ill-posed non-linear problem. Our main contribution is to introduce a material-dependent spatial regularization scheme. The problem is solved iteratively using the Gauss-Newton's method. The framework is validated on numerical experiments of a thorax phantom made of soft tissue, bone and gadolinium scanned with a 90 kV source and a 3-bin photon counting detector.**

I. Introduction

Spectral photon counting detectors [1] can be used to image high Z contrast agents by exploiting the K-edge discontinuity of their energy-dependent linear attenuation coefficient (LAC) [2], [3]. These new scanners open new clinical applications for x-ray imaging as a functional imaging tool, e.g., for the characterization of the atherosclerotic plaque [4].

Spectral CT image reconstruction can be split in two subproblems: (1) decomposition of the energy-resolved data and (2) tomographic reconstruction. The two subproblems can be solved sequentially (projection-based approach) or jointly (image-based approach). Both approaches face challenging difficulties. First, spectral CT is a non-linear problem. Although it can be linearized [5], taking into account the non-linearities of the forward model is more adequate [2]. Second, the sensitivity of spectral imaging is limited [6] and several groups have investigated statistical penalties and spatial priors in the image domain in order to improve the signal-to-noise ratio of the reconstruction [7]–[11].

In this work, we address the basis material decomposition (BMD) problem of the projection-based approach. The main contribution of this work is to introduce a material-specific spatial regularization scheme. Like in [2], our forward model is non-linear and takes into account the spectral response of the detector but we also regularize each material projection image. While the spatial regularization might not be optimal, working on a smaller problem, i.e., one projection at a time, has several advantages: the inverse problem is easier to optimize using explicit computation of sparse matrices, and each problem can be solved in parallel. We present preliminary simulations on synthetic data and the projection of a real thorax phantom.

All authors are with the University of Lyon, INSA-Lyon, Université Lyon 1, CNRS, Inserm, CREATIS UMR 5220 U1206, F-69621, Villeurbanne, France.

F. Peyrin is also with the Synchrotron Radiation Facility, 6 rue Jules Horowitz, F-38043 Grenoble Cedex, France

* nicolas.ducros@creatis.insa-lyon.fr

II. Theory

We consider a 3-dimensional (3-D) object in Ω that is imaged with a 2-D detector with a sensing surface $\mathcal{S}$.

A. Physical models

1) X-ray / matter interactions: Let $n(E, \mathbf{u})$ denotes the number of photons of energy E that reaches the detector at the pixel position $\mathbf{u} \in \mathcal{S}$. Neglecting scattering within the object, n follows the Beer-Lambert law. Mathematically,

$$n(E, \mathbf{u}) = n^0(E) \exp\left[-\int_{\mathcal{L}(\mathbf{u})} \mu(E, \mathbf{x}) \, \mathrm{d}\mathbf{x}\right] \tag{1}$$

where $n^0(E)$ is the source spectrum, $\mathcal{L}(\mathbf{u})$ is the acquisition line that depends on the source emission geometry (parallel, cone-beam, etc), and $\mu(E, \mathbf{x})$ is the local LAC of the object at energy E and point $\mathbf{x} \in \Omega$.

2) Detection model: The signal recorded by a photon counting detector may be modelled by

$$s(\mathcal{E}, \mathbf{u}) = \int_{\mathbb{R}} d(\mathcal{E}, E) \, n(E, \mathbf{u}) \, \mathrm{d}E \tag{2}$$

where $d(\mathcal{E}, E)$ accounts for the detector response function and is the probability density function for an x-ray photon hitting the detector with energy E to be detected at energy $\mathcal{E}$. The photons detected within the ith energy bin $[\mathcal{E}_i, \mathcal{E}_{i+1}]$ are accumulated electronically thanks to a counting circuit. The number of photons detected within the ith energy bin is given by

$$s_i(\mathbf{u}) = \int_{\mathbb{R}} d_i(E) \, n(E, \mathbf{u}) \, \mathrm{d}E \tag{3}$$

where

$$d_i(E) = \int_{\mathcal{E}_i}^{\mathcal{E}_{i+1}} d(\mathcal{E}, E) \, \mathrm{d}\mathcal{E} \tag{4}$$

is the response function of the ith bin of the detector. Note that the detection model assumes that the value measured at a given pixel is not correlated to the value measured at another pixel, i.e. charge sharing can be neglected or is corrected for. It is common to have charge sharing corrected for at the ASIC level.

B. Object decomposition

It is assumed that the LAC is the superposition of M basis functions that are separable in energy and space. We have

$$\mu(E, \mathbf{x}) = \sum_{m=1}^{M} \rho_m(\mathbf{x}) \tau_m(E), \quad \forall \mathbf{x} \in \Omega \tag{5}$$

where the τ_m are some well-chosen basis functions and the ρ_m are the corresponding weights in the decomposition. Following the work of [5], two approaches have emerged for the choice of the basis functions τ_m: i) physics-based where τ_m models the physical effects, e.g. photoelectric, Compton scattering, k-edge, and, ii) material-based where τ_m is the mass attenuation of the constituents of the objects (in $\text{cm}^2.g^{-1}$). Note that in the latter method, ρ_m is the density of material m (in g.cm^{-3}).

C. Forward problem

Substituting (1) and (5) into (3), the measured signal may be written

$$s_i(\mathbf{u}) = \int_{\mathbb{R}} d_i(E) n^0(E, \mathbf{u}) \exp\left[- \sum_{m=1}^{M} a_m(\mathbf{u}) \tau_m(E) \right] \mathrm{d}E \tag{6}$$

where

$$a_m(\mathbf{u}) = \int_{\mathcal{L}(\mathbf{u})} \rho_m(\mathbf{x}) \, \mathrm{d}\mathbf{x} \tag{7}$$

is the projection of the weights ρ_m along the line integral $\mathcal{L}(\mathbf{u})$. When a material-based decomposition is performed, a_m is the mass of the mth material projected onto the detector (in g.cm^{-2}). One main difficulty of the problem we address is the non linearity of the forward mapping expressed in (6).

D. Inverse problem

The detector is assumed to be an array of P pixels centred at $\mathbf{u}_p$, $p \in \{1, \dots, P\}$, and have I energy bins. Let $\mathbf{s} \in \mathbb{R}^{PI}$ be the measurement vector defined by

$$\mathbf{s} = \begin{bmatrix} s_{1,1} & \dots & s_{I,1} & \dots & \dots & s_{1,P} & \dots & s_{I,P} \end{bmatrix}^\top \tag{8}$$

and $\mathbf{a} \in \mathbb{R}^{PM}$ be the (unknown) vector containing the mass of each material in each pixel, which is defined by

$$\mathbf{a} = \begin{bmatrix} a_{1,1} \dots & a_{M,1} & \dots & \dots & a_{M,P} & \dots & a_{M,P} \end{bmatrix}^\top. \tag{9}$$

Our problem is to recover the mass vector $\mathbf{a}$ from the measured data $\mathbf{s}$. This is an ill-posed problem that requires prior knowledge about the solution to stabilize the inversion in the presence of noise.

III. Material and methods

A. Cost function

In this manuscript, we propose to recover the mass vector minimizing the cost function

$$\mathcal{C}(\mathbf{a}) = \|\mathbf{s} - \boldsymbol{\mathcal{F}}(\mathbf{a})\|_2^2 + \alpha \mathcal{R}(\mathbf{a}) \tag{10}$$

where $\boldsymbol{\mathcal{F}}(\mathbf{a})$ is the non-linear forward mapping defined by (6), $\mathcal{R}$ the regularization functional, and α is a global regularization parameter.

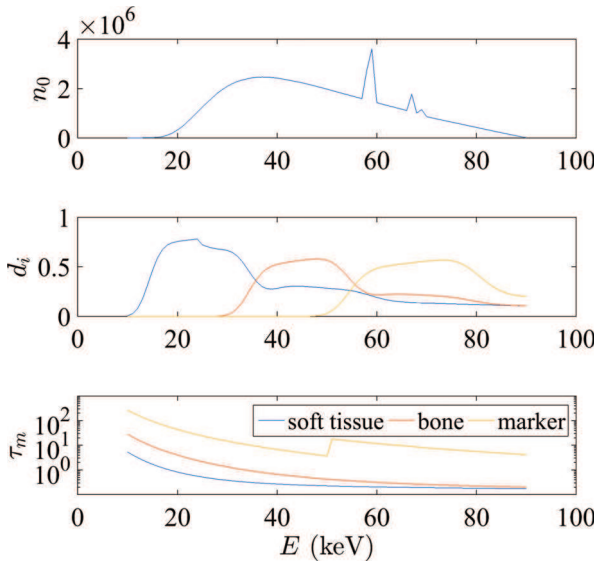

Fig. 1. Spectrum of the x-ray source (top), detector response per bin (middle) and LACs of the three constituents used in the numerical experiments.

B. Regularization functional

We adopt the following regularizing functional, which allows the prior of the different materials to be tuned independently:

$$\mathcal{R}(\mathbf{a}) = \sum_m \alpha_m \mathcal{R}_m(\mathbf{a}_m), \tag{11}$$

where $\mathcal{R}_m$ is the regularizing functional of the mth material weighted by the regularization parameter α_m and $\mathbf{a}_m = [a_{m,1} \dots a_{m,P}]^\top$ is a vector in $\mathbb{R}^P$ that accounts for the mass of the mth material.

C. Optimisation algorithm

We propose to minimize (10) using Gauss-Newton's method, which is a classical iterative tool for non-linear minimization. It starts with an initial guess $\mathbf{a}^{(0)}$ and builds new estimates

$$\mathbf{a}^{(k+1)} = \mathbf{a}^{(k)} + \Delta\mathbf{a}^{(k)} \tag{12}$$

with the so-called Gauss-Newton step $\Delta\mathbf{a}^{(k)}$

$$({\mathbf{J}^{(k)}}^\top \mathbf{J}^{(k)} + \mathbf{H}^{(k)}) \Delta\mathbf{a}^{(k)} = -\mathbf{g}^{(k)}, \tag{13}$$

where $\mathbf{J}^{(k)}$ is the Jacobian matrix of $\boldsymbol{\mathcal{F}}$ about $\mathbf{a}^{(k)}$, $\mathbf{H}^{(k)}$ is the Hessian matrix of $\alpha\mathcal{R}$ about $\mathbf{a}^{(k)}$, and $\mathbf{g}^{(k)}$ is the gradient of $\mathcal{C}$ about $\mathbf{a}^{(k)}$.

D. Numerical simulations

1) Acquisition parameters: We consider the source spectrum $n_0(E)$ that is depicted on the top row of figure 1. It was obtained with a tube voltage of 90 kV. Measurements were performed in $I = 3$ energy bins. The response function of each bin is plotted in the middle row of figure 1 and was taken from [2] (3 out of 8 bins). The measurements were corrupted by Poisson noise assuming 10^8 x-ray photons are launched onto the patient towards each each pixel of the detector. We

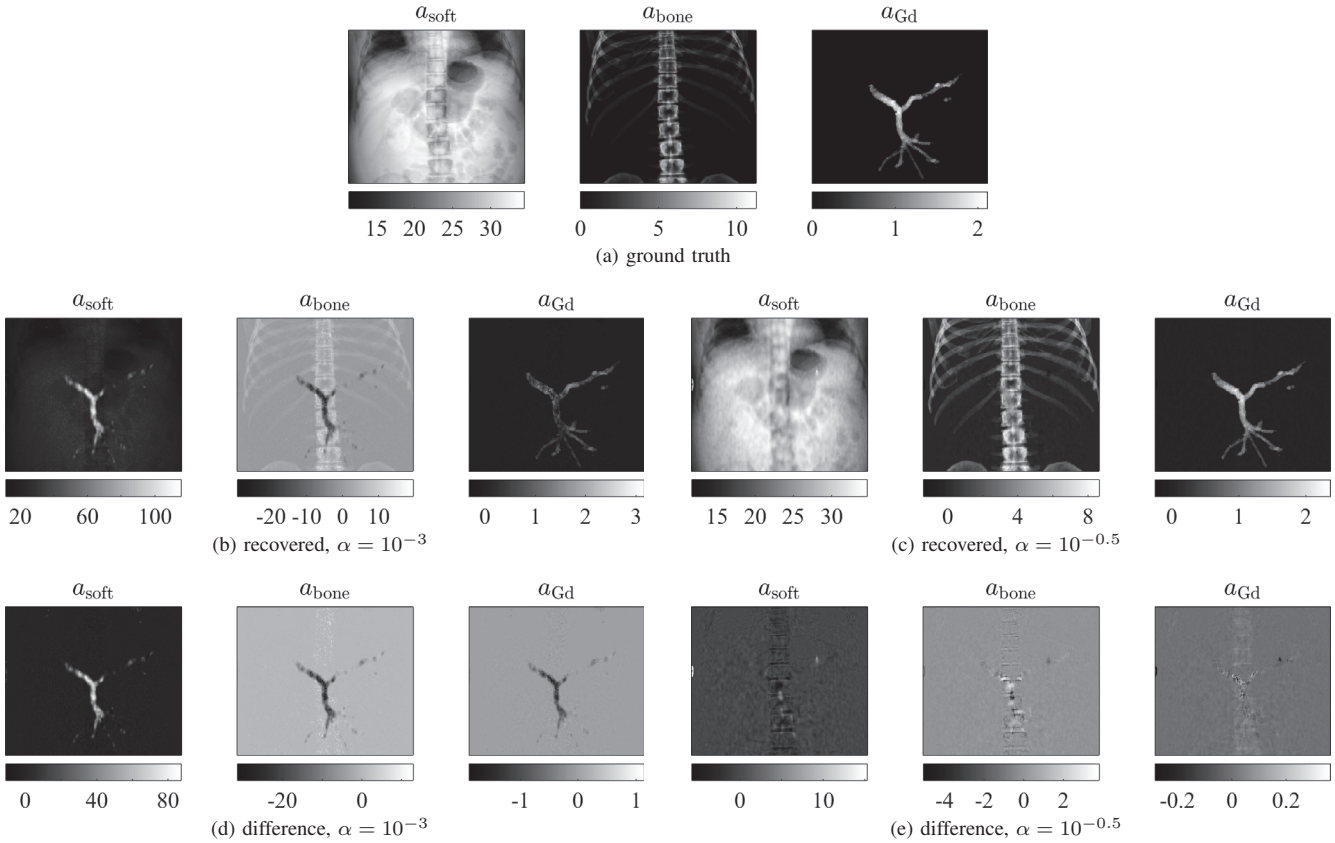

Fig. 2. Mass of the constituents of the phantom in units of g.cm^{-2}, namely soft tissue, bone, and gadolinium. a) ground truth images, b) recovered images for a small regularization parameter, c) recovered images for the best regularization parameter, d) difference between b) and a), and e) difference between c) and a).

approximated this Poisson noise to a Gaussian distribution and the square L_2 norm chosen in this work is effective as a data fidelity term.

2) Phantom: We considered the 3D thorax phantom that was segmented from a CT scan in [12]. Each voxel has been associated to either soft tissue or bone, according to the segment it belongs to. The material density in each voxel was estimated from the CT images. The portal vein was marked with gadolinium at a concentration of 1 g.cm^{-3}. The mass attenuations of soft tissue, bone, and gadolinium were taken from ICRU report 44 [13] and are depicted in figure 1 (bottom row). The projected masses for each material are finally computed according to (7), by integrating densities along parallel lines chosen perpendicular to the coronal plane. The resulting material images are displayed on the top row of figure 2.

3) Spatial regularization: For this 3-material phantom, we choose

$$\alpha\mathcal{R}(\mathbf{a}) = \alpha\left(\|\Delta\mathbf{a}_{\text{soft}}\|_2^2 + \|\nabla\mathbf{a}_{\text{bone}}\|_2^2 + \|\nabla\mathbf{a}_{\text{Gd}}\|_1\right) \quad (14)$$

where $\mathbf{a}_{\text{soft}}$, $\mathbf{a}_{\text{bone}}$, and $\mathbf{a}_{\text{Gd}}$ represents the projected masses of soft tissues, bone, and gadolinium, respectively, while ∇ and Δ are the first- and second-order differential operators, respectively. This functional promotes solutions for which i) the soft tissue and bone images are smooth, ii) the marker image is piecewise constant, and iii) the soft tissue image is smoother than the bone image. As a first approach, we set $\alpha_m = 1$ for each of the material images, keeping only the global regularization parameter as a free parameter. To compute $\mathbf{H}^{(k)}$ and $\mathbf{g}^{(k)}$, a smooth approximation of the ℓ_1-norm is considered, namely the pseudo-Huber loss function [14].

IV. Results

The cost function given by (10) was minimized iteratively by a Gauss-Newton algorithm according to (12) and (13). The algorithm is initialized with the uniform material images $\mathbf{a}_{\text{soft}}^{(0)}$ = 20 g.cm^{-2}, $\mathbf{a}_{\text{bone}}^{(0)}$ = 2 g.cm^{-2}, and $\mathbf{a}_{\text{Gd}}^{(0)}$ = 0 g.cm^{-2}. The algorithm is stopped when the cost function decrease is less than 0.1%. The minimization was performed for different regularization parameters α ranging from 10^{-2} and 10^{1}. For our 361×167 images, updating $\mathbf{a}^{(k)}$ took 2 s on a standard laptop (2.6 GHz i7 CPU and 16 GiB of RAM). Depending on the regularization parameter, from 15 to 30 iterations were necessary before convergence, which leads to a computation time of about 30 to 60 s to minimize (10).

The plot of the points $(\|\mathbf{s} - \boldsymbol{\mathcal{F}}(\mathbf{a})\|_2^2, \mathcal{R}(\mathbf{a}))$ for different values of the regularization parameter α, which is known as the L-curve, is provided in figure 3. The reconstruction error $\|\mathbf{a} - \mathbf{a}_{\text{true}}\|_2 / \|\mathbf{a}_{\text{true}}\|_2$ is displayed with respect to α in figure 4. The smallest reconstruction error was obtained for $\alpha = 10^{-0.5}$, which corresponds to the corner of the L-curve,

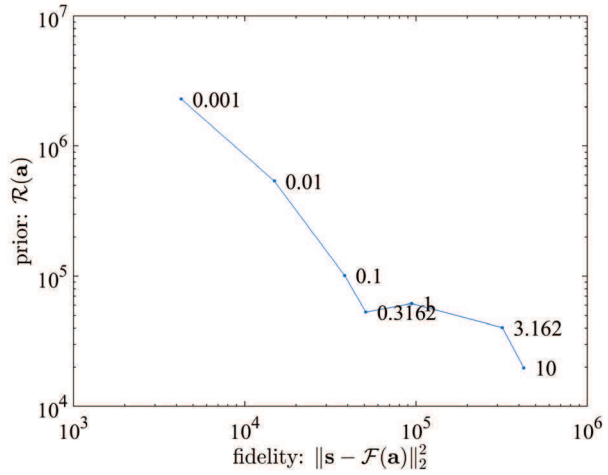

Fig. 3. L-curve for the proposed experient, i.e., $(\|\mathbf{s}-\boldsymbol{\mathcal{F}}(\mathbf{a})\|_2^2, \mathcal{R}(\mathbf{a}))$ for a regularization parameter α ranging from 10^{-2} to 10^{1}.

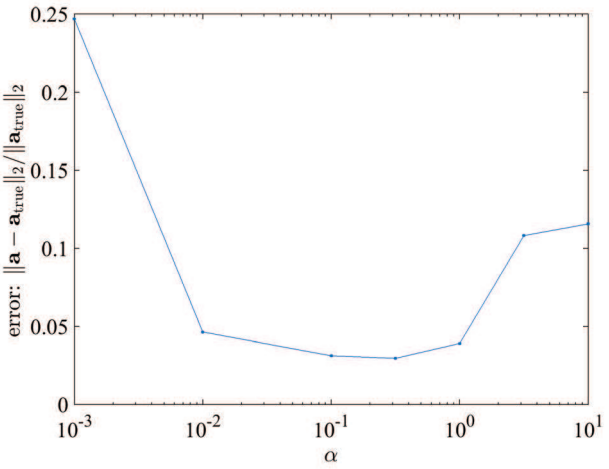

Fig. 4. Decomposition error with respect to regularization parameter.

indicating than the L-curve may be an appropriate tool for selecting the regularization parameter when the ground truth is unknown. The material images recovered by our method are given in the middle row of figure 2. Two regularization parameters were considered, one being very small (left) and the other being the best one according to the L-curve (right). When no regularisation scheme is used (see figures 2b and 2d), the different materials are poorly separated. However, the three material images are nicely recovered when an appropriate regularization scheme is considered.

V. Discussion and Conclusion

These preliminary results indicate that the decomposition of x-ray spectral projection images greatly benefits from the implementation of a regularization scheme. Similar results have been reported in the image domain but working in the projection domain is advantageous because the dimensionality is smaller and, therefore, more tractable. For example, we have been able to compute the L-curve in figure 3, which might not be tractable considering the image-based approach.

We have used a single regularization parameter in this work. Future works include the use of several regularization parameters. We will also investigate other statistical methods that better accounts for the statistical noise in the projection images and other regularizations, e.g., a non convex prior for the gadolinium favoring a small support. After a satisfying solution has been developed in the projection domain, a set of projection images can be decomposed and reconstructed using existing filtered-backprojection or iterative CT reconstruction algorithms.

Acknowledgment

This work was partly supported by the grant ANR-11-INBS-0006 and by the grant ANR-13-IS03-0002-01 (DEXTER project) of the French National Research Agency (ANR). It was also performed within the framework of the LABEX PRIMES (ANR-11-LABX-0063) of Université de Lyon, within the program ANR-11-IDEX-0007.

References

[1] K. Taguchi and J. S. Iwanczyk, "Vision 20/20: Single photon counting x-ray detectors in medical imaging," *Medical Physics*, vol. 40, no. 10, p. 100901, 2013.

[2] J. P. Schlomka, E. Roessl, R. Dorscheid, S. Dill, G. Martens, T. Istel, C. Bumer, C. Herrmann, R. Steadman, G. Zeitler, A. Livne, and R. Proksa, "Experimental feasibility of multi-energy photon-counting k-edge imaging in pre-clinical computed tomography," *Physics in Medicine and Biology*, vol. 53, no. 15, p. 4031, 2008.

[3] C. Schirra, B. Brendel, M. Anastasio, and E. Roessl, "Spectral CT: a technology primer for contrast agent development," *Contrast Media Mol Imaging*, vol. 9, no. 1, pp. 62–70, 2014.

[4] D. P. Cormode, E. Roessl, A. Thran, T. Skajaa, R. E. Gordon, J.-P. Schlomka, V. Fuster, E. A. Fisher, W. J. M. Mulder, R. Proksa, and Z. A. Fayad, "Atherosclerotic plaque composition: Analysis with multicolor ct and targeted gold nanoparticles1," *Radiology*, vol. 256, no. 3, pp. 774–782, 2010.

[5] R. E. Alvarez and A. Macovski, "Energy-selective reconstructions in x-ray computerised tomography," *Physics in Medicine and Biology*, vol. 21, no. 5, p. 733, 1976.

[6] E. Roessl, B. Brendel, K. Engel, J. P. Schlomka, A. Thran, and R. Proksa, "Sensitivity of photon-counting based k -edge imaging in x-ray computed tomography," *Medical Imaging, IEEE Transactions on*, vol. 30, no. 9, pp. 1678–1690, 2011.

[7] C. Schirra, E. Roessl, T. Koehler, B. Brendel, A. Thran, D. Pan, M. Anastasio, and R. Proksa, "Statistical reconstruction of material decomposed data in spectral ct," *Medical Imaging, IEEE Transactions on*, vol. 32, no. 7, pp. 1249–1257, 2013.

[8] Y. Long and J. Fessler, "Multi-material decomposition using statistical image reconstruction for spectral ct," pp. 1–1, 2014.

[9] A. Sawatzky, Q. Xu, C. Schirra, and M. Anastasio, "Proximal admm for multi-channel image reconstruction in spectral x-ray ct," pp. 1–1, 2014.

[10] Q. Xu, A. Sawatzky, M. A. Anastasio, and C. O. Schirra, "Sparsity-regularized image reconstruction of decomposed k-edge data in spectral ct," *Physics in Medicine and Biology*, vol. 59, no. 10, p. N65, 2014.

[11] R. Zhang, J.-B. Thibault, C. Bouman, K. Sauer, and J. Hsieh, "Model-based iterative reconstruction for dual-energy x-ray ct using a joint quadratic likelihood model," *Medical Imaging, IEEE Transactions on*, vol. 33, no. 1, pp. 117–134, Jan 2014.

[12] R. Kechichian, S. Valette, M. Desvignes, and R. Prost, "Shortest-path constraints for 3d multiobject semiautomatic segmentation via clustering and graph cut," *Image Processing, IEEE Transactions on*, vol. 22, no. 11, pp. 4224–4236, Nov 2013.

[13] ICRU, "Report 44 of the tissue substitutes in radiation dosimetry and measurement," International Commission on Radiation Units and Measurements (ICRU), Tech. Rep., 1989.

[14] P. Charbonnier, L. Blanc-Feraud, G. Aubert, and M. Barlaud, "Deterministic edge-preserving regularization in computed imaging," *IEEE Trans Image Process*, vol. 6, no. 2, pp. 298–311, 1997.